3D Relativistic Hydrodynamics

Miguel A. Aloy[1] and José M. Martí[2]

[1] Max-Planck-Institut für Astrophysik,
Karl-Schwarzschild-Str. 1, 85748 Garching, Germany
[2] Departamento de Astronomía y Astrofísica, Universidad de Valencia,
C/ Doctor Moliner 50, 46100 Burjassot, Spain

Abstract. We review the evolution of the numerical techniques applied in relativistic hydrodynamics since the sixties until today. We focus our attention on the state–of–the–art high–resolution shock–capturing methods and the astrophysical applications involving three–dimensional simulations.

1 Introduction

A relativistic description of fluid dynamics is necessary in situations where the local velocity of the flow is close to the light speed in vacuum (c) or where the local internal energy density is comparable (or larger) than the local rest–mass density of the fluid. Alternatively, a relativistic description should be used whenever matter is influenced by large gravitational potentials ($\approx O(c^2) \approx 9\,10^{20}$ erg g^{-1}), where a description in terms of the Einstein field theory of gravity is necessary. Relativistic flows are present in numerous astrophysical phenomena, from stellar to galactic (and even cosmological –early Universe, galaxy formation–) scales. Among these phenomena are core collapse supernovae, X-ray binaries, pulsars, coalescing neutron stars and black holes, micro-quasars, active galactic nuclei, superluminal jets, gamma-ray bursts and, in general, any astrophysical scenario involving compact objects.

More than thirty years ago, the pioneering work of May and White [103], studying the process of stellar core collapse in spherical symmetry, triggered the use of relativistic numerical simulations as a tool to get insight into the above mentioned phenomena, complementing theoretical models and observations. However, the description of the ultrarelativistic regime has only been possible after the development, in the last ten years, of new numerical algorithms (the so called high–resolution shock–capturing, HRSC, techniques).

This work is aimed to summarize the basic theory of the numerical techniques applied to solve multidimensional (specifically three-dimensional, 3D) problems in the frame of relativistic hydrodynamics (RHD). Recent works reviewing this topic are [102] (in Special Relativity) and [45] (in General Relativity). In addition, we discusse the state of art of the current numerical 3D RHD codes. The work is organized as follows. The equations of General Relativistic Hydrodynamics (GRHD) are introduced in §2. Some important mathematical properties of the GRHD equations (conservative character, hyperbolicity) are discussed in Sections 2.1 and 2.2. Section 2.3 points out briefly the main differences between

classical and relativistic equations. Sections 3, 4 and 5 form the body of the review. Section 3 is devoted to discuss different approaches for the integration of the RHD eqs. paying special attention to the most recent numerical algorithms. Present numerical 3D RHD codes are reviewed in §4 as well as some computational issues relevant for three dimensional simulations. Several astrophysics applications are discussed in §5. We finish this work with a summary (6).

2 The equations of General Relativistic Hydrodynamics

The equations that describe the evolution of a relativistic fluid can be written as covariant divergences,

$$\nabla \cdot \mathbf{J} = 0 \,, \tag{1a}$$

$$\nabla \cdot \mathbf{T} = 0 \,, \tag{1b}$$

representing the conservation of rest-mass and energy–momentum in the space–time $\mathcal{M}$, described by a metric $\mathbf{g}$. In the previous equations, $\mathbf{J}$ is the current of rest mass and $\mathbf{T}$ is the energy-momentum tensor. For perfect fluids (*i.e.,* those without shear or heat conduction) and using a system of natural units ($G = c = 1$; G is the gravitational constant), the components of $\mathbf{J}$ and $\mathbf{T}$ on a coordinate basis are

$$J = \rho u^\mu \,, \qquad \mu, \nu = 0, \ldots, 3 \tag{2a}$$

$$T^{\mu\nu} = \rho h u^\mu u^\mu + p g^{\mu\nu} \,, \tag{2b}$$

ρ, p, h, ε and u^μ being the rest–mass density, the pressure, the specific enthalpy ($h = 1 + \varepsilon + p/\rho$), the specific internal energy and the four–velocity of the fluid, respectively. The system of equations (1a, 1b) is closed making use of the normalization condition of the four velocity ($u^\mu u_\mu = -1$, where summation is extended over repeated indices) and an equation of state (EoS), usually of the form $p = p(\rho, \varepsilon)$.

A consistent numerical simulation of the flow evolution within the framework of Relativity requires, in principle, the solution of the RHD equations (relativistic counterparts of the Euler or Navier–Stockes equations) coupled to the *full* set of Einstein field equations (that control the evolution of the space–time). However, the problem is so complex (especially in multidimensions), and the variety of astrophysical phenomena is so wide that for practical purposes it is worthy to consider different physical approximations. The easiest one is to consider that the gravitational field is unimportant and, therefore, the space–time is flat or, in other words, the metric of the space–time is the Minkowski metric. This is the approach of Special Relativistic hydrodynamic (SRHD) simulations and has been successfully applied to, *e.g.,* extragalactic jets (*e.g.,* [101]), afterglows of gamma–ray bursts (GRBs) [122], and also in other fields of physics, like *e.g.,* relativistic heavy–ion collisions [150]. Another possibility is to assume that the simulated flow is a *test fluid* evolving in an external static field created

by a massive object. This is the approximation followed in most GRHD problems. The GRHD approximation is fruitfully used in simulations of accretion of matter onto compact objects [63] and also in the context of the formation of GRBs [7] (see § 5.2). However, when strong and varying gravitational fields are encountered, the evolution of the metric has to be obtained by solving the Einstein field equations (EFE). This situation holds, *e.g.,* in the case of coalescing neutron stars (NSs) [86] or in the collapse of a massive star to a black hole (BH) – *e.g.,* [103] –.

2.1 Equations of GRHD in conservation form

Following the {3+1} formalism [9], and given a general coordinate system $\{x^\mu\} \equiv (t, x^i)$, the space–time $\mathcal{M}$ can be foliated into a set of spacelike hypersurfaces Σ_t (for each constant value of t) such that

$$\partial_t = \alpha \mathbf{n} + \beta^i \partial_i, \quad \mathbf{n} \cdot \partial_i = 0, \quad i = 1, 2, 3,$$

where $\{\partial_t, \partial_i\}$ define a coordinate basis and $\mathbf{n}$ is the unit timelike vector field normal to Σ_t.

The line element on $\mathcal{M}$ may be written in terms of the scalar *lapse*, α, the *shift* vector, β^i, and the three–metric of each hypersurface Σ_t, γ_{ij},

$$ds^2 = -(\alpha^2 - \beta_i \beta^i) dt^2 + 2\beta_i dx^i dt + \gamma_{ij} dx^i dx^j.$$

In coordinates $\{x^\mu\}$, equations (1a, 1b) are written (in conservation form) as

$$\frac{1}{\sqrt{-g}} \left[\frac{\partial \sqrt{\gamma} \mathbf{U}(\mathbf{W})}{\partial t} + \frac{\partial \sqrt{-g} \mathbf{F}^{(i)}(\mathbf{W})}{\partial x^i} \right] = \mathbf{S}(\mathbf{W}), \tag{3}$$

where g stands for the determinant of the four–metric of $\mathcal{M}$ and γ for the determinant of γ_{ij}, and where $\mathbf{U} \equiv (D, S_j, \tau)$ is the vector of unknowns, which are the rest-mass, momentum and energy densities, respectively, as measured by Eulerian observers (i.e., those having $\mathbf{n}$ as four–velocity). In the previous equations $\mathbf{F}^{(i)}$ are the vectors of fluxes

$$\mathbf{F}^{(i)}(\mathbf{W}) = \left[D \left(v^i - \frac{\beta^i}{\alpha} \right), S_j \left(v^i - \frac{\beta^i}{\alpha} \right) + p \delta^i_j, \tau \left(v^i - \frac{\beta^i}{\alpha} \right) + p v^i \right]$$

and $\mathbf{S}$ is the vector of sources

$$\mathbf{S}(\mathbf{W}) = \left[0, \; T^{\mu\nu} \left(\frac{\partial g_{\nu j}}{\partial x^\mu} - \Gamma^\delta_{\nu\mu} g_{\delta j} \right), \; \alpha \left(T^{\mu 0} \frac{\partial \ln \alpha}{\partial x^\mu} - T^{\mu\nu} \Gamma^0_{\nu\mu} \right) \right] .$$

Conserved variables are related with physical or *primitive* variables, $\mathbf{W} \equiv (\rho, \varepsilon, v^i)$, i.e., the rest-mass density and specific internal energy in the fluid rest frame and the fluid three–velocity measured by Eulerian observers, respectively, through

$$D = \rho \Gamma \tag{4a}$$

$$S_j = \rho h \Gamma^2 v_j \quad (j = 1, 2, 3) \tag{4b}$$

$$\tau = \rho h \Gamma^2 - p - \rho \Gamma, \tag{4c}$$

where

$$v_i = \frac{\mathbf{u}\cdot\partial_i}{-\mathbf{u}\cdot\mathbf{n}}$$
$$v^i = \gamma^{ij}v_j = \frac{u^i}{\alpha u^t} + \frac{\beta^i}{\alpha}\,,$$

and $\Gamma \equiv -\mathbf{u}\cdot\mathbf{n} = (1-\gamma_{ij}v^iv^j)^{-1/2}$ is the Lorentz factor.

2.2 GRHD equations as a hyperbolic system of conservation laws

Following, *e.g.*, [157], a system of q equations written in *conservation form*, like (3), is said to be hyperbolic at a point (t, x^i) if the Jacobian matrices of $\mathbf{F}^{(i)}$ ($\mathcal{B}^{(i)} = \partial\mathbf{F}^{(i)}/\partial\mathbf{U}$) have p real eigenvalues $\lambda_1,\ldots,\lambda_q$ and corresponding sets of p linearly independent right eigenvectors $\mathbf{r}^{(1)},\ldots,\mathbf{r}^{(q)}$.

The characteristic curves associated to the system are (in the one–dimensional case) the integral curves of

$$\frac{dx}{dt} = \lambda_k(\mathbf{U}(x,t)),\ \ k = 1,\ldots q \tag{5}$$

where we can notice that the eigenvalues of $\mathcal{B}^{(i)}$ are the velocities of propagation of the characteristic fields (characteristic speeds). Along each characteristic curve, there is one characteristic variable, *i.e.*, a component of $\mathcal{U}^{(i)} = \mathbf{L}^{(i)}\mathbf{U}$ ($\mathbf{L}^{(i)}$ is the matrix of left eigenvectors of $\mathcal{B}^{(i)}$), which remains constant. This fact allows one to construct formally solutions at advanced times by propagating the values of characteristic variables at previous times along the characteristic curves, i.e., by solving initial value problems (IVPs).

Anile [8] has shown that system (3) is hyperbolic for causal EoS, *i.e.*, for those where the local sound speed, c_s, defined by

$$hc_s^2 = \frac{\partial p}{\partial\rho} + (p/\rho^2)\frac{\partial p}{\partial\epsilon}, \tag{6}$$

satisfies $c_s < 1$.

In the particular case of SRHD the set of eigenvalues associated to the Jacobian matrix in the i–direction are [43,35,3]

$$\lambda_0 = v^i, \tag{7a}$$
$$\lambda_\pm = \frac{1}{1-v^2c_s^2}\left(v^i(1-c_s^2) \pm c_s\sqrt{(1-v^2)[1-v^2c_s^2-v^iv^i(1-c_s^2)]}\right). \tag{7b}$$

Let us notice that: (i) there exists a strong coupling between the components of velocity along the different spatial directions through the modulus of the velocity, v; (ii) in the one–dimensional case (1D) the expressions of $\lambda_\pm$ (associated to the acoustic waves) reduce to the Lorentz addition of the flow velocity and the local sound speed

$$\lambda_\pm = \frac{v \pm c_s}{1 \pm vc_s}; \tag{8}$$

(iii) $\lambda_\pm \rightarrow v \pm c_s$ in the Newtonian limit ($v, c_s \rightarrow 0$), and $\lambda_\pm \rightarrow 1$ in the ultrarelativistic limit ($v \rightarrow 1$).

For the sake of completeness let us say that the eigenvalues and right eigenvectors corresponding to the Jacobian matrices of fluxes in system (3) appear explicitly in ref. [12]. The explicit expression of the left eigenvectors can be found in ref. [3].

An important property of hyperbolic systems of conservation laws is that they admit discontinuous solutions (shocks). These discontinuous solutions satisfy the Rankine-Hugoniot (RH) jump conditions which establish the continuity of mass, momentum and energy fluxes across shocks. In the case of SRHD these conditions [154] read:

$$[\rho u^\mu] r_\mu = 0 \,, \tag{9}$$

$$[T^{\mu\nu}] r_\mu = 0 \,, \tag{10}$$

r_μ being the unit normal to the hypersurface of the space–time, σ, containing the discontinuity. The square brackets define the jump of a given variable across σ ($[F] = F_a - F_b$; where F_a, F_b are the values of F on the two sides of σ).

Considering σ as normal to the x-axis, a suitable choice of r_ν is $r^\nu = \Gamma_s(V_s, 1, 0, 0)$, where V_s is interpreted as the coordinate velocity of the hypersurface that defines the position of the shock wave and $\Gamma_s = (1 - V_s^2)^{-1/2}$ is the Lorentz factor associated to the shock.

RH conditions (9), (10) can be written in terms of the conserved and primitive quantities and the invariant mass flux across the shock, j ($j \equiv \Gamma_s D_a \{V_s - v_a^x\} = \Gamma_s D_b \{V_s - v_b^x\}$),

$$[v^x] = -\frac{j}{\Gamma_s} \left[\frac{1}{D}\right], \tag{11}$$

$$[p] = \frac{j}{\Gamma_s} \left[\frac{S^x}{D}\right], \tag{12}$$

$$\left[\frac{S^{y,z}}{D}\right] = 0, \text{ or } [h\Gamma v^{y,z}] = 0, \tag{13}$$

$$[v^x p] = \frac{j}{\Gamma_s} \left[\frac{\tau}{D}\right]. \tag{14}$$

Equation (13) implies that the orientation of the tangential velocity does not change across shocks. This also holds for selfsimilar expansions or rarefaction waves. However, the values of the components of the tangential velocity, (v^y, v^z), may jump across the shock (contrary to Newtonian hydrodynamics). In the case of contact discontinuities (no mass flux across the discontinuity, $j = 0$) arbitrary jumps in the tangential velocity are allowed although pressure and normal velocity should be continuous.

2.3 Newtonian versus Relativistic Hydrodynamics

The classical Euler equations are easily recovered from the RHD equations in the limit $c \to \infty$. The limits of the conserved variables and flux vectors lead to the corresponding quantities in the classical case:

$$\mathbf{U} = (D, S^j, \tau) \qquad \to (\rho, \rho v^j, \frac{1}{2}\rho \mathrm{v}^2 + \rho\varepsilon)$$

$$\mathbf{F}^{(i)} = (Dv^i, S^j v^i + p\delta^{ji}, S^i - Dv^i) \to (\rho v^i, \rho v^j v^i + p\delta^{ji}, v^i(\frac{1}{2}\rho \mathrm{v}^2 + \rho\varepsilon + p))$$

$$i, j = 1, 2, 3$$

The equations keep their conservative and hyperbolic characters but there are several factors that make RHD more complex to solve numerically than classical hydrodynamics: (i) the RHD equations are tightly coupled through Γ and h and, therefore, they display a larger non-linearity; (ii) there is no explicit relation between $\mathbf{W}$ and $\mathbf{U}$ (except for particular EoS), *i.e.,* obtaining the primitive from the conserved variables needs an iterative numerical method; (iii) the tangential flow velocity can change across discontinuities (see § 2.2) and, in addition, the characteristic speeds may suffer from aberration (see the coupling between different directions in expression (7b)); (iv) in the ultrarelativistic limit ($v \to 1$), the eigenfields are degenerate ($\lambda_0 \to \lambda_\pm \to 1$) which triggers the appearance of very thin structures in the flow (like, *e.g.,* in the case of relativistic blast waves) that may become a source of numerical errors; and (v) relativistic strong shocks can display unbounded jumps in physical variables; *e.g.,* for an ideal gas (*i.e.,* with an EoS: $p = (\gamma - 1)\rho\varepsilon$), the compression ratio between the post– and pre–shocked densities of a relativistic strong shock is such that (see, *e.g.,* [155]) $\rho_b/\rho_a \leq (\gamma\Gamma_a + 1)/(\gamma - 1)$ which tends to infinity in the ultrarelativistic limit ($v_a \to 1$). This should be compared with the compression ratio in a Newtonian strong shock: $\rho_b/\rho_a \leq (\gamma + 1)/(\gamma - 1)$ which is $\sim 4 - 7$ for typical values of γ.

3 Numerical integration of the RHD equations

The first attempts to solve numerically the equations of RHD started in the late 60's [103]. Since then and up to the 80's the field has been dominated by the so called artificial viscosity (AV) techniques. This was the result of the application of von Neumann & Richtmyer's [162] ideas (in the framework of classical hydrodynamics) to RHD. Basically, the algorithms consisted of standard finite difference techniques together with *viscous* terms added to the equations to damp spurious oscillations near shocks. The AV terms were *non–consistent* because they were not based on the energy–momentum tensor of a viscous fluid. However, they provide an artificial dissipative mechanism that makes the shock transition smooth, *i.e.,* extended over several numerical zones. The approach needs a large dissipation (the amount of viscosity being problem dependent) to handle strong relativistic shocks and, therefore, AV schemes may be very diffusive (smearing out every discontinuity in the flow). In addition, the algorithms were not

conservative and, hence, did not guarantee the propagation of discontinuities at the correct (physical) velocities. Due to all these problems, traditional AV methods are not optimal both in the mildly and in the ultrarelativistic regimes (*i.e.*, $\Gamma \geq 2$).

Over and above all these considerations, it remains true that AV methods have been widely used in many fields of astrophysics and we summarize briefly some of their key contributions. The first 1D, Lagrangian, full GRHD code (*i.e.*, also evolving the EFE) corresponds to May & White [103] and it was applied to stellar core collapse. However, due to the Lagrangian character of the code, it was impossible to extend it to multidimensions. Another important improvement was made by Wilson during the 70's [164,165]. In ref. [164] he presented the first multidimensional (2D), Eulerian, full GRHD numerical code. This code (and some different versions of it) has been successfully applied to axisymmetric stellar collapse (*e.g.*, [127,151,148,114,111,40]), accretion onto compact objects (*e.g.*, [63,125]) and numerical cosmology (*e.g.*, [24]).

As an example of the performance of the methods, we reproduce in Fig. 1b the plot given by Norman & Winkler [118] showing the evolution of the relative errors of Centrella & Wilson's algorithm [24] for the case of the reflection of a mildly relativistic shock against a wall (see Fig. 1a for a schematic representation). The solution develops a shock that moves away from the wall. In the postshock state the gas is at rest and much hotter than the gas in the preshocked medium. It is noticeable from Fig. 1b that errors are larger than 5% even for values of Γ as small as $\simeq 2.3$.

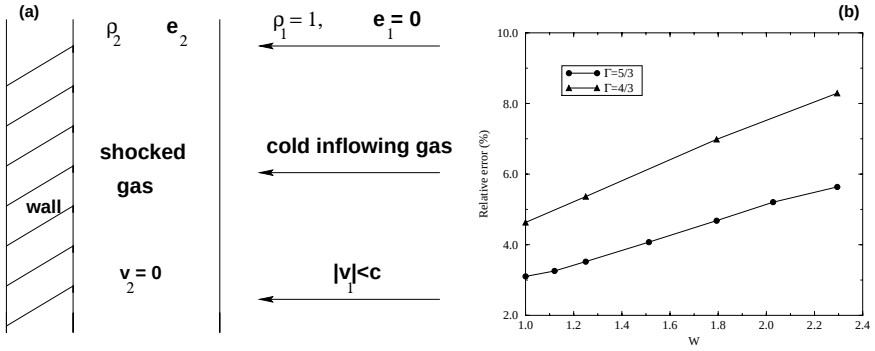

Fig. 1. (**a**) Scheme of the relativistic shock reflection test. (**b**) Relative errors of the relativistic shock reflection test as a function of the Lorentz factor (W in the plot) of the inflowing gas for two different values of the adiabatic index (Γ in the plot legends) using the explicit Eulerian techniques of [24]. Data from Centrella and Wilson [24]. Plot reproduced from Norman and Winkler [118].

In the mid eighties, Norman & Winkler [118] proposed a reformulation of the difference equations with artificial viscosity consistent with the relativistic

dynamics of non-perfect fluids. Accurate results across strong relativistic shocks with large Lorentz factors were obtained in combination with adaptive mesh techniques. However, the strong coupling introduced in the equations by the presence of the viscous terms in the definition of relativistic momentum and total energy densities required an implicit treatment of the difference equations and prevented the extension of the algorithm to multidimensions.

During the 1990's, a major break-through in the simulation of ultrarelativistic flows was accomplished when high–resolution shock–capturing (HRSC) methods, specially designed to solve hyperbolic systems of conservation laws, were applied to solve the RHD equations. Their application has caused a revolution in numerical RHD because (i) writing the equations in conservation form, guarantees convergence to the physically correct solution; (ii) HRSC methods exploit the hyperbolic character of the RHD equations and, therefore, the solution automatically satisfies RH conditions (this is the reason why they are called *shock–capturing*); and (iii) they provide high resolution in the sense that they have high order of accuracy in smooth regions of the flow while keeping discontinuities stable and sharp.

3.1 Basic procedure of HRSC methods

As in any finite difference or finite volume scheme, the first step consists in discretizing the equations on a finite numerical grid (t^n, x_j)

$$x_j = (j - 1/2)\Delta x, \quad j = 1, 2, \dots , \tag{15}$$

$$t^n = n\Delta t, \quad n = 0, 1, 2, \dots , \tag{16}$$

Δt, Δx being the time step and the zone size, respectively. The discretization of the system is such that the time evolution of zone averaged state vectors, $\mathbf{U}_j^n$, is governed by functions called *numerical fluxes*, $\hat{\mathbf{F}}_{j\pm1/2}$, evaluated at zone interfaces:

$$\frac{d\mathbf{U}_j^n}{dt} = -\frac{1}{\Delta x}\Big(\hat{\mathbf{F}}_{j+1/2}(\mathbf{U}_{j-r}^n, \mathbf{U}_{j-r+1}^n, \dots, \mathbf{U}_{j+q}^n) - \hat{\mathbf{F}}_{j-1/2}(\mathbf{U}_{j-r-1}^n, \mathbf{U}_{j-r}^n, \dots, \mathbf{U}_{j+q-1}^n)\Big) .$$

where p and q are positive integers. Usually, $\mathbf{U}_j^n$ is an approximation to the zone average of $\mathbf{U}$ defined by

$$\mathbf{U}_j^n = \frac{1}{\Delta x}\int_{x_{j-1/2}}^{x_{j+1/2}} \mathbf{U}(t^n, x)dx , \tag{17}$$

which is consistent with the integral form of the system of conservation laws and, $\hat{\mathbf{F}}_{j\pm1/2}$ are the time–averaged fluxes across the interfaces $x_{j\pm1/2}$ ($x_{j\pm1/2} = (x_j + x_{j\pm1})/2$) :

$$\hat{\mathbf{F}}_{j\pm1/2} \approx \frac{1}{\Delta t}\int_{t^n}^{t^{n+1}} \mathbf{F}(\mathbf{U}(t, x_{j\pm1/2}))dt . \tag{18}$$

Computation of numerical fluxes. Numerical fluxes must be consistent with the actual fluxes, *i.e.,* $\hat{\mathbf{F}}(\mathbf{U},\mathbf{U},\ldots,\mathbf{U}) = \mathbf{F}(\mathbf{U})$. In (18) the only unknown is the value of the solution at every cell interface, $\mathbf{U}(t, x_{j\pm1/2})$ and its dependence on time. There are several ways of calculating (18), that give rise to different HRSC schemes. One of the most fruitful subset of methods are called *Godunov–type methods* (because they were first used in Godunov [51]). The discretization procedure approximates the solution by a piecewise continuous function at each time step (see Fig. 2 bottom panel) and, therefore, at every cell interface a jump between adjacent zone averaged values may occur. The situation is such that locally (at each interface) at every time level, t^n, one has an IVP with piecewise constant initial data for the RHD equations, *i.e.,* a Riemann problem (RP; see, *e.g.,* [157]). In Godunov-type methods, $\mathbf{U}(t, x_{j\pm1/2})$ is calculated by solving these RPs at every zone interface. The exact solution of the RP for the Euler equations is known (*e.g.,* [30] and references therein) and consists of a set of constant states separated by centered rarefactions, contact discontinuities and/or shocks connecting the piecewise constant *left* and *right* states. The top panel of Fig. 2 shows a space–time diagram of the evolution of the solution at several adjacent cell interfaces. The time step between two consecutive time levels, t^n, t^{n+1} must be limited in order to prevent the interaction of the solution of adjacent interfaces. This restriction on dt is known as Courant–Friedrich–Lewi (CFL) condition.

High order of accuracy. In order to understand the meaning of *high resolution* we need to introduce some mathematical concepts (see, *e.g.,* [87] for details). We say that the solution converges under grid refinement when the global error $||E_{\Delta x}||$, defined as

$$||E_{\Delta x}|| = \Delta x \sum_j |\bar{\mathbf{U}}_j^n - \mathbf{U}_j^n|, \tag{19}$$

tends to zero as $\Delta x \to 0$ ($\bar{\mathbf{U}}_j^n$ is the average of the *true* solution in the cell j). The idea behind definition (19) is that the finer the grid is, the better the numerical solution. Lax equivalence theorem [133] asserts that stability is a necessary condition to guarantee convergence. A measure of the stability of a solution can be its total variation at $t = t^n$, $\mathrm{TV}(\mathbf{U}^n)$, defined as

$$\mathrm{TV}(\mathbf{U}^n) = \sum_{j=0}^{+\infty} |\mathbf{U}_{j+1}^n - \mathbf{U}_j^n| \,. \tag{20}$$

A numerical scheme is said to be TV–stable, if $\mathrm{TV}(\mathbf{U}^{n+1}) \leq \mathrm{TV}(\mathbf{U}^n)$, $\forall n$ for any initial data. For non–linear, scalar conservation laws, a numerical scheme converges if it is written in conservation form with consistent numerical flux functions, and if it is TV–stable [87].

High–order accuracy in smooth parts of the flow is achieved by using conservative monotonic polynomial functions to interpolate the approximate solution within numerical cells. The reason to choose monotonic functions is that

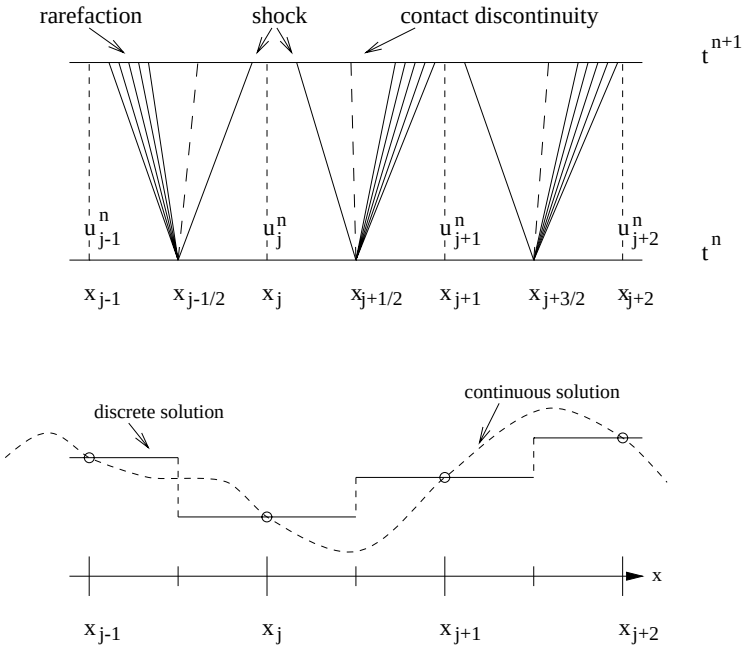

Fig. 2. Godunov's scheme: local solutions of Riemann problems. At every interface, $x_{j-\frac{1}{2}}$, $x_{j+\frac{1}{2}}$ and $x_{j+\frac{3}{2}}$, a local Riemann problem is set up as a result of the discretization process (bottom panel), when approximating the numerical solution by piecewise constant data. At time t^n these discontinuities decay into three elementary waves which propagate the solution forward to the next time level t^{n+1} (top panel). The time step of the numerical scheme must satisfy the Courant-Friedrichs-Lewy condition, being small enough to prevent the waves from advancing more than $\Delta x/2$ in Δt.

they lead to a decrease of the total variation of the solution (total–variation–diminishing schemes, TVD; [61]), ensuring stability. This interpolation or cell reconstruction provides more accurate left and right states for the Riemann problem by substituting the mean values $\mathbf{U}_j^n$ (that produces only first–order accuracy) by better representations of the true flow near the interfaces, thereupon, new RPs are setup at each cell interface. Different choices of the interpolation polynomial lead to TVD schemes of different order of accuracy. Piecewise constant functions provide first order accuracy (this was the original method of Godunov [51]). Second order of accuracy is obtained if piecewise linear functions are used (*e.g., monotonic upstream scheme for conservation laws* – MUSCL – method [158]) and, piecewise parabolic functions provide third order accuracy (*piecewise piecewise method* – PPM – [28]). Albeit it is possible to construct higher order polynomials to obtain better accuracy in smooth parts of the flow, it should be remarked that TVD methods degenerate to first order accuracy at extrema [119]. Therefore, other types of reconstruction (not being TVD) have been developed like, *e.g.,* total –variation–bounded (TVB) schemes [146], the *essen-*

tially non–oscillatory (ENO) schemes [62] and the *piecewise–hyperbolic method* (PHM) [93]. In other approaches, like the FCT algorithm (see, *e.g.*, [20]), a high order of accuracy is obtained by adding an anti–diffusive flux to a first order accurate numerical flux.

Time advance. There are two main procedures to advance the conserved variables in time. One possibility is a standard discretization of the time derivative in system (17). In this case, the accuracy of the method depends on the order of accuracy up to which the numerical fluxes have been computed. The second alternative (known as the method of lines) regards (17) as a semidiscrete (*i.e.*, spatially discretized) system of ordinary differential equations to which any standard ordinary differential equation solver (*e.g.*, a Runge Kutta solver) can be applied.

3.2 Riemann Solvers

The key ingredient of Godunov–type methods is the solution of the RP at zone interfaces. Nevertheless, there is no exact closed–form to the RP neither for the RHD equations nor for the classical Euler equations, not even for ideal gases. Iterative algorithms are devised whereby the solution can be computed numerically up to any practical degree of accuracy. Numerical schemes aimed to solve RPs are known as Riemann solvers.

The solution of the RP can be either exact or approximate and, therefore, the Riemann solvers can be, at first instance, classified as exact or approximate Riemann solvers. Although the exact solution to the RP is known, there are a number of reasons to compute approximate solutions. The first is that the precision of any difference method is finite and, actually depends on the order of the method. Hence, an approximate RP solution with an accuracy better than that of the finite difference scheme might be acceptable. The second reason is that exact Riemann solvers are computationally expensive algorithms while approximate ones are more efficient. That is particularly important in multidimensional calculations because then numerical efficiency is a main issue. Finally, the solution of the RP is averaged in time to compute the numerical fluxes (see 18) and, therefore, the fine details of the solution are lost. Hence, it may pay off to evaluate an approximate (but accurate enough) solution to the RP.

Among the class of exact Riemann solvers, Godunov [51] is credited with the first exact Riemann solver for the Euler equations. Martí & Müller [98] extended this classical solution of the RP to the SRHD equations when the velocities parallel to the initial discontinuity (tangential velocities) are zero. Pons, *et al.* [130] have given the general solution (for non–vanishing tangential velocities) for the RP in SRHD. Wen, Panaitescu & Laguna [163] have extended Glimm's method or Random Choice Method [50,25] to 1D SRHD. Balsara [11] and Dai & Woodward [31] have extended to SRHD the two–shock approximation method of Colella [27] for classical fluid dynamics.

The strategy to construct approximate Riemann solvers (in both classical and relativistic hydrodynamics) relies on the local linearization of the Jacobian

matrices of the flux vectors, $\mathcal{B}^{(i)}$, extending a procedure introduced by Roe [132] and sometimes referred to as *local characteristic approach* (LCA). The idea of the LCA is to use the spectral decomposition of $\mathcal{B}^{(i)}$ to rewrite the original system as a new one of uncoupled scalar equations, in terms of the characteristic variables. The locally linear system can then be easily solved to obtain appropriate numerical fluxes for the original system. Sometimes the linearization process involves an averaged intermediate state at zone interfaces. This is the case of the original Roe solver [132] and its relativistic extension [39], and Martí *et al.* [97] or Falle & Komissarov [41] approaches. Donat & Marquina [36] have extended a numerical flux formula which was first proposed by Shu & Osher [147] for scalar equations to systems. In the scalar case and for characteristic wave speeds which do not change sign zone interfaces, Marquina's flux formula is identical to Roe's flux. Otherwise, the scheme switches to the more viscous, entropy satisfying local Lax–Friedrichs scheme [147]. In the case of systems, the combination of Roe and local–Lax–Friedrichs solvers is carried out in each characteristic field after the local linearization and decoupling of the system of equations [36]. However, contrary to Roe's and the previously cited linearized methods, the extension of Marquina's method to systems does not require on any averaged intermediate state. Marquina's flux formula has been successfully used in the ultrarelativistic regime and in 2D axisymmetric [100,101] and 3D SRHD [3] and even in 3D GRHD [7,44].

Finally, a very simple approach is an extension of the Harten, Lax, van Leer (HLL) solver to SRHD [139]. This method avoids the explicit calculation of the eigenvalues and eigenvectors of the Jacobian matrices and is based on an approximate solution of the original Riemann problems with a single intermediate state, $\mathbf{U}_*$, determined by requiring consistency of the approximate Riemann solution with the integral form of the conservation laws in a grid zone. The algorithm needs estimates of lower and upper bounds for the smallest and largest signal velocities, $a_{\rm L}$ and $a_{\rm R}$, respectively. Good estimates for $a_{\rm L}$ and $a_{\rm R}$ are essential to guarantee robustness and, at the same time, the minimal amount of numerical viscosity (the larger the difference $||a_{\rm L}| - |a_{\rm R}||$ is, the larger the viscosity of the method; if the difference is too small, undesired numerical oscillations around discontinuities appear). In the non-relativistic case, Einfeldt [37] proposed to use the smallest and largest eigenvalues of Roe's matrix (this corresponds to the HLLE solver). Duncan & Hughes [33] have generalized the method to 2D SRHD.

3.3 Other HRSC schemes

Symmetric TVD schemes with nonlinear numerical dissipation. Symmetric TVD (sTVD) methods [32] are another subset of the HRSC methods. As Godunov–type methods, they are written in conservation form, but they are not based on solving Riemann problems. sTVD methods use standard finite difference methods (*e.g.,* Lax Wendroff scheme) and employ local conservative dissipation terms in order to stabilize the algorithm across discontinuities. The numerical dissipation term is local, free of problem dependent parameters and does not require any characteristic information. Hence, they are simpler than

Godunov–type schemes. Extensions to 2D and 3D general relativistic magneto hydrodynamics (GRMHD) can be found in, *e.g.*, [74,73,116].

Relativistic beam scheme. In the *beam scheme* [136] and its relativistic extension [167] the hydrodynamic equations are solved as the limit of the corresponding Botzmann equation. The velocity distribution functions are approximated by several Dirac delta functions or discrete beams of particles in each computational cell, which reproduce the appropriate moments of the distribution functions. This beam scheme, although being a particle method derived from a microscopic kinetic description, has all the desirable properties of modern characteristic–based wave propagation methods based on a macroscopic continuum description. Yang *et al.* [167] show that the integration scheme for the beams can be cast in the form of an upwind conservation scheme in terms of numerical fluxes and build up high–order variants of the relativistic code in terms of different TVD and ENO interpolations.

3.4 Other approaches.

Van Putten's approach. Van Putten [159] solves the equations of (ideal) special relativistic magneto–hydrodynamics (SRMHD) formulating Maxwell's equations as a hyperbolic system in divergence form. State vectors and fluxes are decomposed into a spatially constant mean and a spatially dependent variational part. Then, the SRMHD equations become an evolution system for integrated (continuous) quantities for which standard integration methods can be used. In order to update the state vectors of the original system, a numerical differentiation of the integrated quantities is necessary. This process can lead to oscillations in the case of strong shocks and a smoothing algorithm needs to be supplied. The approach has been applied to SRMHD jets with values of the Lorentz factor up to 4.25 [160,161].

Relativistic Smoothed Particle Hydrodynamics. Smoothed particle hydrodynamics (SPH; [89]) represents a fluid by a Monte Carlo sampling of its mass elements. The motion and thermodynamics of these mass elements is governed by the hydrodynamic equations. As the equations involve continuous properties of the fluid, it is necessary to estimate these quantities from the positions, velocities and internal energies of the fluid mass elements, which are like particles moving with the flow. SPH treats the particle positions as a finite set of interpolating points where the continuous fluid variables and their gradients are estimated by an appropriately weighted average over neighboring particles. This means that it is a free–Lagrange method, *i.e.*, spatial gradients are evaluated without the use of a computational grid. As a result, the method provides a genuinely multidimensional (3D) description of the fluid with a lower computational cost (depending on the number of particles employed) than typical finite volume, HRSC, multidimensional methods. SPH has been extended to SRHD by Monaghan [109]. Other SRHD applications can be found in, *e.g.*, [84,91,92,26].

Implementations of SPH in GRHD may be seen in [70,83,145]. The artificial viscosity (necessary to handle discontinuities in the fluid) is the most critical issue for relativistic SPH codes. The reason is that, unlike its Newtonian analogue, the relativistic theory has not yet been developed to the degree required to predict – by a relativistic kinetic theory – the form of the dissipation terms. To overcome this problem, the most successful approach consists on taking the concepts from Riemann solvers as a guide to improve the artificial viscosity required in SPH (see [110,26]).

4 Computational issues and current 3D RHD codes

4.1 Computational issues

Due to the extreme computational resources demanded by typical 3D RHD simulations – as compared to 1D or 2D RHD ones –, technical improvements of the codes are required. Among the most important issues that should be addressed we find the optimization of the memory and the algorithm itself and, the design of suitable strategies for data analysis.

Memory handling optimization. Even small problems in 3D require huge amounts of RAM memory. As an example, 15 variables (e.g., a set of five conserved variables, five primitive variables and five fluxes) discretized in a volume containing 256^3 cells, in double precision ($\times 8$ bytes), would need ~ 2 Gb of RAM. Moreover, this number of 3D variables is a very moderate value that can easily be multiplied by a factor of ~ 4 if a GRHD problem with dynamical evolution of the space–time is considered, or if several chemical species are present in the fluid. Thereby, a reduction towards the minimal set of 3D variables is mandatory. In addition, the algorithms should be designed to allow for an efficient memory access (which is a computer dependent issue), the reason being that nowadays the speed of the memory systems is about one order of magnitude smaller than the actual CPU speeds. This last point is particularly critical when superscalar, cache–oriented computers (the most commonly used systems in supercomputing, at present) are used. Finally, high order methods are preferred in 3D, because less grid points are needed to resolve fine structures in the fluid (as compared with lower order methods).

Algorithm optimization. A typical 3D RHD code, using an ideal EoS, may need about 10^{-4} s to update a numerical zone on a single processor. If one has to update 256^3 zones, the time per code iteration is roughly 30 minutes per processor. This means that 1000 time steps may need several days to a few weeks to be completed. This time estimate, can grow drastically if, *e.g.,* realistic microphysics and/or EoS are used. Hence, code efficiency becomes important in order to reduce the total computational time. An obvious way of decreasing the run time is to simplify analytically all the expressions, in particular those that may lead to numerical cancellation errors [5]. However, the largest impact

on performance comes from computer architecture considerations, *i.e.*, it is necessary to write algorithms oriented to the type of computer that is going to be used (cache based, vector based, etc.). Code parallelization and/or vectorization is unavoidable to work on current (both distributed or shared memory based) supercomputers. Finally, given that the affordable resolution in *fixed* 3D grids is still far from being appropriate to study many problems – even with the largest supercomputers –, resolution enhancement algorithms are crucial (like, *e.g.*, adaptive mesh refinement [15], multiresolution [60]).

Data analysis. Applying the same data analysis than in 1D or 2D it is neither appropriate nor feasible in 3D, the reason being the huge data sets to be stored (an analyzed). A crude estimate of the typical storage requirements necessary to save every variable at every time step leads to unpractical (if not at all affordable) values of the order of terabytes of disc space. Albeit, it is convenient to design *a priori* the analysis strategy, *i.e.*, it is convenient to choose which variables have to be saved. An example of this kind of procedure is the synthesis of emission maps from simulations of relativistic jets including time–delay effects (see Sect. 5). In such a case, the values of the state variables in many different time levels are necessary in order to integrate the emission along rays parallel to the line of sight (for a given observing angle). In practice the number of time levels required to make the full integration is of the same order than the number of time steps of the simulation, which means that terabytes of data should be saved. An alternative is to choose *a priori* the viewing angles that are interesting and perform the integration on run time – picking out the values from the appropriate zones at each time level for every angle –.

4.2 Technical status of the existing 3D RHD codes

There are, according to our knowledge, four different 3D RHD codes, used in astrophysical applications: Koide–Nishikawa's code [74,76], GENESIS [3], Cactus [44] and Shibata–Nakamura's code [143]. In the following we will describe some of the main features of each one.

The group of Koide and coworkers has developed a GRMHD code (for a fixed background metric) based on a sTVD scheme (see Sect. 3.3). The code has been applied to study the propagation of extragalactic jets through magnetized atmospheres [115] and also to simulate the early stages of jet formation by magnetohydrodynamic mechanisms in background BH spacetimes [75]. A series of tests of Koide et al.'s method involving mainly continuous solutions can be found in ref. [76]. Koide et al.'s code has proven to be very stable (although very difussive) when simulating mildly relativistic flows (maximum Lorentz factors ≈ 4) with discontinuities.

GENESIS [3] is a conservative 3D RHD code (used in astrophysical SRHD and GRHD applications) based on HRSC techniques. It uses Marquina's flux formula to compute numerical fluxes and a third order PPM spatial interpolation. The time advance is performed by means of a high–order Runge–Kutta method.

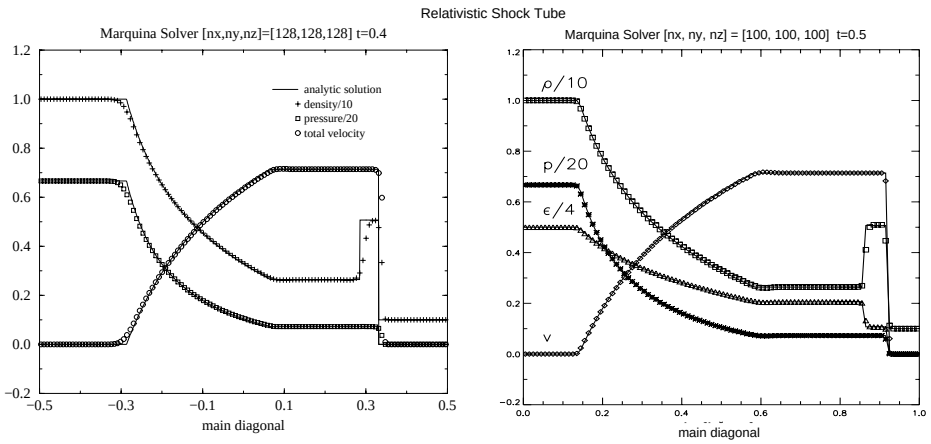

Fig. 3. Comparative performance of Cactus (left panel; figure from [44]) and GENESIS (right panel; figure from [3]) on a three–dimensional mildly relativistic shock tube test. The panels show several primitive variables along the main diagonal of the computational domain (solid line: analytic solution; symbols: numerical solution). The initial data are a constant left (L) and right (R) state characterized by $(\rho_L, p_L, v_L) = (10, 13.3, 0)$ and $(\rho_L, p_L, v_L) = (1, 0.66 \cdot 10^{-6}, 0)$. Numerical grid and evolution time is similar in both cases.

GENESIS has been extensively tested in problems involving strong shocks even in the ultrarelativistic regime, being able to handle Lorentz factors as large as $3 \cdot 10^5$ (in the one–dimensional wall reflection test). Simulations of extragalactic jets (using SRHD, at both parsec [6] and kiloparsec [4] scales) and progenitors of GRBs (in GRHD with a Schwarzschild background metric, [7]) have been performed with GENESIS.

Cactus is a numerical tool developed within a collaboration of the Numerical Relativity divisions at the National Center for Supercomputing Applications, the Albert Einstein Institut and the Washington University [22]. Cactus is able to solve the full set of Einstein field equations coupled to a perfect fluid source. The hydrodynamic evolution employs HRSC methods and can be computed by means of different Riemann solvers (Roe, Marquina) and flux–splitting schemes. The metric evolution may be followed with several formalisms (ADM, hyperbolic formulations, conformal–tracefree) combined with a number of integration methods (leapfrog, Crank–Nicholson, MacCormack along with Strang splitting) and various gauges (algebraic, maximal slicing, etc.). The main goal of the code is the simulation of astrophysical processes involving NSs and BHs. Font *et al.* [44] have tested the capabilities of the hydro part computing shock tubes. In Fig. 3, a comparison between Cactus and GENESIS is shown for a mildly relativistic Riemann problem. Despite the slightly different grids (100^3 for GENESIS, 128^3

for Cactus) the results are still comparable, the reason being that both codes use the same HRSC techniques. Font *et al.* [44] have also tested the GRHD coupling in Cactus simulating Friedman–Robertson–Walker cosmologies with dust and polytropic NSs (static and boosted). Alcubierre *et al.* [2] have performed a number of experiments (Brill waves, single BH, static boson and neutron stars) comparing different formulations of the Einstein equations. Recently, Landry & Teukolsky [86] have performed simulations of coalescing binary NSs. The stability of the Einstein evolution is a main issue of this code, especially when the ADM or hyperbolic formulations are considered.

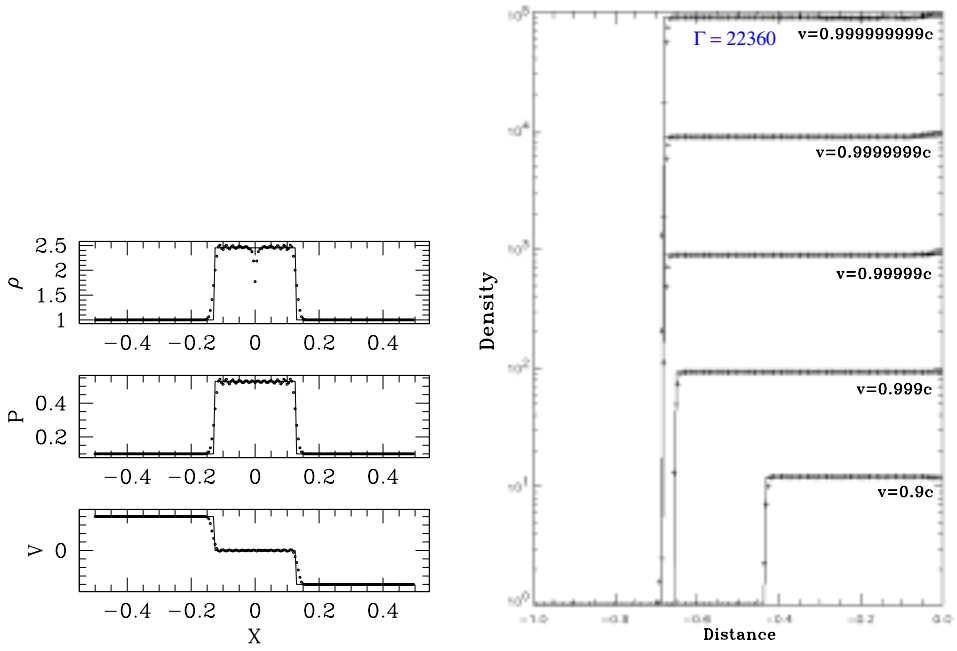

Fig. 4. Comparative performance of Shibata–Nakamura' code (left panel; figure from [143]) and GENESIS (right panel; figure from [3]) on the shock reflection test. In both cases the abscissas represent the distance to the reflection point. Left panel shows, from top to bottom, the density, pressure and flow velocity distributions, for an inflow velocity of $0.4c$. In the right panel, the density distribution (in logarithmic scale) is shown for a sample of inflow velocities –from $0.9c$ to $0.999999999c$–.

Shibata–Nakamura's code is based on the conformal–tracefree (CT) formulation of the Einstein equations [141,140,142]. The hydrodynamic equations are

written (and solved) as a set of advection (i.e., non–conservative) equations to which AV is added as in Wilson's traditional approach (see § 3). The CT formulation is employed for the Einstein equations which are evolved by means of a leapfrog scheme. Several gauges are available (maximal slicing, minimum distortion). Shibata & Nakamura [140] have used this code to study the gravitational wave production of selected matter configurations. Rigidly rotating neutron star stability and neutron star mergers in 3D were computed in [113,143]. For the first time in 3D full GR, the dynamical collapse of a rotating neutron star has been simulated with this scheme [144]. Although the code –and the CT formulation– allows for the longest stable evolutions in dynamical space–times, the quality of the results, as measured by the degree of fulfillment of the constraint Einstein equations, is not as satisfactory as in the ADM or hyperbolic formulations. A comparison between the quality of the results of Shibata–Nakamura's code and GENESIS (using HRSC methods) is shown in Fig. 4 for the shock reflection test in a flat space–time. Shibata & Nakamura' results (for an inflow velocity as small as $0.4c$) display the well known pathologies of traditional relativistic AV methods in the treatment of shocks (diffusion, oscillations). HRSC techniques are much less diffusive (even with Lorentz factors as large as 22360) and produce more stable profiles in the postshock state.

5 Applications

In this Section we will review briefly some of the most relevant 3D applications of SRHD and SRMHD codes in astrophysical scenarios (i.e., relativistic jets) as well as recent GRHD and GRMHD simulations in the context of progenitors of GRBs and jet formation, respectively. Applications to dynamical space–times, in which Einstein equations are coupled to the GRHD equations, are beyond the scope of this article (for a review see, *e.g.*, [45]).

5.1 Relativistic astrophysical jets

In the standard model [19,138] the elongated radio structures connected to the center of AGNs in radio galaxies and radio–loud quasars are considered as continuous ejections of highly collimated, supersonic and very stable plasma. The emission is produced by synchrotron and inverse Compton processes of electrons accelerated up to ultrarelativistic energies in the vicinity of a *central engine*. The asymmetries in the radio flux of the two oppositely directed jets of a source and the superluminal motions observed in a few dozens of compact sources are explained by assuming that both jets propagate with relativistic speeds along directions at small angles to the line of sight. The relativistic Doppler beaming of the emission in the direction of motion accounts for the observed emission asymmetries whereas apparent superluminal speeds are explained by the combination of a finite value of the speed of light and the relativistic motion of the emitting source.

The formation, collimation and propagation of extragalactic jets involves scales ranging from some microparsecs to hundreds of kiloparsecs. Thereby, the study of the jet phenomenon is conveniently chopped into several pieces each one covering a smaller range of length scales. The mechanism governing the jet formation and collimation is still a challenge, mainly because the most detailed high–frequency VLBI observations of nearby radio sources can resolve at most the compact radio cores with a linear resolution of ≥ 0.1 pc [17] [1], while the Schwarzschild radius ($R_s = GM/c^2$) of a $10^9 M_\odot$ galactic BH (the supposed central engine in the most commonly accepted interpretation) is $\sim 10^{-5}$ pc. Consistently, our theoretical view of jet formation is mainly constrained by the fact that many jets are well collimated by the time they have propagated to a distance $\leq$ 1pc from the nucleus (*e.g.*, [69]). Several mechanisms of jet formation have been proposed, all of which present some difficulties [13]. Additionally, there is a wide variety in the observed properties of jets, so there may be a variety of jet collimation mechanisms. The standard model assumes that jet formation involves accretion onto a central compact object, such as a NS or a stellar BH in the case of galactic microquasars (GRS 1915+105 [107] and GRO J1655-40 [156]), or a supermassive BH in AGNs. This accretion fuels bipolar outflows which are further collimated and accelerated by MHD processes at subparsec scales (see, *e.g.*, [81]).

At parsec scales (from 0.1 pc to 100 pc) jets are observed using VLBI imaging. VLBI radio maps display highly collimated jets whose morphology is characterized by a bright spot at the jet end and a series of components which separate from the core, sometimes at superluminal speeds. Many parsec scale jets show intraday variability of the radio flux, excess in brightness temperatures and one-sidedness. The interpretation of these features is that the jet material moves at small angles to the line of sight with bulk Lorentz factors $\Gamma \simeq 15 h_{65}^{-1}$ [49] (h_{65} is Hubble's constant in units of 65 km/s Mpc^{-1}), or even larger ($\Gamma \simeq 30 - 100$) if the intraday variability is intrinsic and a result of incoherent synchrotron radiation [14]. The moving components are interpreted, within the *shock–in–jet* model as traveling shock waves [95,54]. A worthy byproduct of this model is the explanation of the complex multifrequency brightness and polarization variations in blazars.

At kiloparsec scales, sources are shaped by the interaction with the external medium, with a morphological dichotomy between FRI and FRII [42] sources whose basis seems to be the source power. The morphology of FR I sources is the result of a deceleration from relativistic to non–relativistic, transonic speeds [16,85], occurring within the first kpc. In the case of the FRIIs, mildly relativistic jet speeds (Lorentz factors between 2 and 3) well outside the galaxy have been inferred from flux asymmetries between jets and counter–jets [21] and superluminal motions at kpc scales (*e.g.*, in 1928+738 [65] and 1055+201, 1830+285, 2209+080 [64]). The mechanism by which the relativistic flows inferred from radio jets at pc scales remain collimated up to kpc scales is still unresolved.

[1] The VLBI Space Observatory Program (VSOP), allows for a linear resolution of $\sim 0.1 - 1$ pc even in distant sources like S5 0836+710 ($z = 2.17$; [88]).

Large scale jets. At far enough distances from the central object (pc and kpc scales) the effects of gravity are negligible and we can assume (as a first approximation to the problem) that magnetic fields are dynamically unimportant. In this approach, numerical simulations using a pure SRHD treatment have been performed since the early 90s to study the morphology and dynamics of relativistic jets.

The development of codes based on HRSC techniques has allowed 2D axisymmetric time–dependent relativistic hydrodynamic simulations [33,38,99–101,80,134] to be performed. These simulations led to the conclusion that both the internal energy and the Lorentz factor of the beam enhance the stability of relativistic jets compared to their classical counterparts, through the increase of the effective inertial mass of the beam. Relativistic MHD simulations in 2D using pseudo–spectral techniques [159,161] or sTVD methods [74,73] have been another step forward in our understanding of relativistic astrophysical jets.

Only since 1998 the morphology and dynamics of relativistic jets is studied with 3D SRHD [3,4] or SRMHD [115,116] simulations. Aloy *et al.* [3] did a 3D simulation (in Cartesian coordinates) of an axisymmetric relativistic jet propagating through an homogeneous atmosphere. The simulated jet is characterized by a beam–to–external proper rest–mass density ratio $\eta = 0.01$, a beam Mach number $\mathcal{M}_b = 6.0$, and a beam flow speed $v_b = 0.99c$. An ideal gas equation of state with an adiabatic exponent $\gamma = 5/3$ is assumed to describe both the jet matter and the ambient gas. The beam is in pressure equilibrium with the ambient medium which fills a domain (X,Y,Z) with a size of $15R_b \times 15R_b \times 75R_b$ ($120 \times 120 \times 600$ cells), where R_b is the beam radius. The jet is injected at $z = 0$ in the direction of the positive z-axis through a circular nozzle. Simulations were typically performed with 16 R10000 processors (on a SGI-Origin 2000) and need about ten thousand time iterations. The execution time was about 100 hours. Genuine multidimensional effects were included by perturbing the axial injection velocity.

Koide and collaborators [115,116] simulated the evolution of relativistic jets through a magnetized uniform atmosphere during a very brief period of time. The numerical setup [116] consisted on a cylindrical jet injected through a circular nozzle into an oblique (45° with respect to the jet axis) magnetic atmosphere. The computational domain was a cubic box of $20R_b \times 20R_b \times 20R_b$ ($101 \times 101 \times 101$ cells). The jet had the following parameters: $v_b = 0.98756c$, ratio between the beam and magnetic specific energy densities $\varepsilon_b/\varepsilon_m = 1/3$, $\mathcal{M}_b = 4.0$, $\gamma = 5/3$ and considered two different strengths for the ambient magnetic field, *weak* and *strong*. The simulation lasted for 35 CPU hours on a SGI–Power Challenge and required about 1 Gb of RAM. It should be remarked that the coarse grid zoning used in Nishikawa's [116] simulations (5 cells/R_b), prevented them from studying genuine 3D effects in relativistic jets in detail.

Parsec scale jets. The presence of emitting flows at almost light speed enhances the importance of relativistic effects in the apparency of jets. This fact is stressed in the case of parsec scale jets, triggering the combination of syn-

chrotron emission models and hydrodynamic simulations to compare with observations. Theoretical models aimed at explaining the appearance of radio jets [68,94,95,72] studied the spectrum of the synchrotron emission produced in different parts of the jet and the perturbations induced on the spectrum due to jet inhomogeneities. The inhomogeneities were introduced to mimic the ejection of components in real sources. The (frequency dependent) light curves of both total and polarized flux of the ejected components are understood as enhanced emission behind relativistic shock waves propagating down the underlying steady jet (*shock–in–jet* model).

The theoretical models gave rise to more detailed numerical models (see, *e.g.,* [67,96,53]) which, however, were restricted to a simplified (one-dimensional) hydrodynamic evolution. In 1995, Gómez *et al.* [55] produced the first numerical simulations of the pc scale synchrotron emission from 2D SRHD jets. Since then, other works have followed the same approach [56,34,106,79].

Very recently, Aloy *et al.* [6] have computed, for the first time, the emission from 3D relativistic jets. As in the previous 2D simulations, the approach followed by Aloy et al. rested on two main points. First the jet structure is calculated using a relativistic time–dependent hydrodynamic code. Second, the radio emission from the hydrodynamic jet models is computed by integrating the transfer equations of synchrotron radiation, once the appropriate relations between the computed hydrodynamic quantities and the emission/absorption coefficients are established. The procedure accounts for the appropriate opacity and relativistic effects, such as Doppler boosting and relativistic aberration. The simulations were done with the code GENESIS [3] and the radio emission was calculated with the same code as in Gómez *et al.* [55,56] (see also [58]). Aloy *et al.* [6] discuss some observational consequences of the interaction between the relativistic jet and the surrounding medium, leading to the development of a shear layer. The presence of such a layer (with distinct kinematic properties and magnetic field configuration) has been invoked *ad hoc* in the past by several authors [78,85] to account for a number of observational characteristics in FR I radio sources. However, its physical nature is still largely unknown. Remarkable effects associated with this layer are, *e.g.,* the presence of rails of low polarization intensity (see emission dips in Fig. 5–right) along the shear layer. Recently, Swain, Bridle, & Baum [152] have found evidence of such shear layers in FR II radio galaxies (3C353), and Attridge, Roberts, & Wardle [10] have inferred a two-component structure in the parsec scale jet of the source 1055+018.

Jet formation Within the framework of General Relativity, GRMHD 2D axisymmetric simulations of early phases of jet formation from magnetized accretion disks around a non–rotating (Schwarzschild) BH [76] or rotating (Kerr) BH [77] have been performed, assuming a fixed background metric. The magnetic stress induced by the axial magnetic field anchored to the disk (in Keplerian rotation) is responsible of the angular momentum loss of the disk material, triggering the accretion process. In the non–rotating Schwarschild BH case [76] a jet is formed with a maximum velocity of $0.93c$ ($W = 2.7$) if a hydrostatic corona is

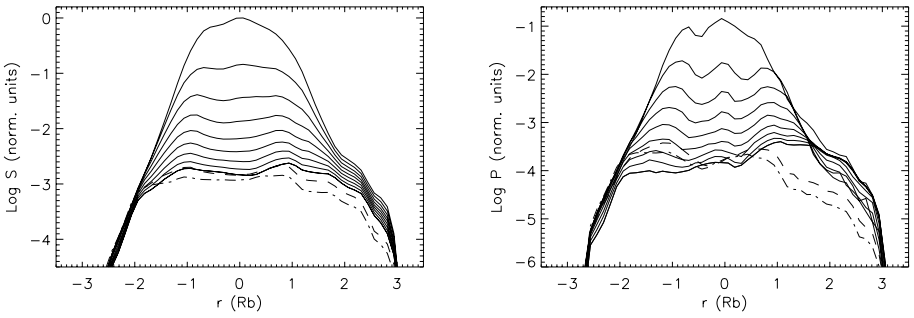

Fig. 5. Figure from [6]. Logarithm of the integrated total (*left*) and polarized (*right*) intensity across the jet for different viewing angles. Lines are plotted in intervals of 10° from an angle of 10° (top line in both plots), to 90° (showing a progressive decrease in emission). Dashed lines (dot dashed) correspond to an observing angle of -100° (-140°). Units are normalized to the maximum in total intensity.

considered and with a maximum velocity of $0.4c$ if a free falling corona embedding the black hole is assumed. A two layered jet structure (in agreement with theoretical predictions – *e.g.*, [18] –) is found. The inner part is pressure driven and moves at relativistic speeds in the hydrostatic corona case. The outermost part is magnetically driven and subrelativistic. This shell structure might be the origin of the shear layer mentioned in the previous section. Nevertheless, for a fast rotating BH [77], the maximum velocities obtained are $0.4c$ (counter–rotating disk) and $0.3c$ (co–rotating disk), and again the two layered outflow structure is formed (see Fig. 6). As the simulations had to be stopped due to numerical problems quite early [77], the total evolution time was not large enough to develop highly relativistic jets. Therefore, despite of the promising results of Koide's group, the mechanism of jet formation still remains an open and challenging question (see, *e.g.*, [135]).

5.2 Gamma–ray bursts

GRBs are known observationally since over 30 years [71]. They consist of very short, non–repeating events (except for a few soft gamma–ray repeaters), with a typical duration between several milliseconds and several hundreds of seconds, showing a large variability even at millisecond scale. They show a bimodal time–distribution, the border between the two groups being at ~ 2 s. The first group is composed of *short* bursts centered around 0.1 s, while the second group consists of *long* bursts (more numerous and softer than the first group) centered at about 15 s. The time–structure is very different from burst to burst.

GRB spectra are non–thermal. The observed energy flux as a function of the energy can be well described by one or a combination of several power laws. The maximum of the energy distribution corresponds to an energy (the energy

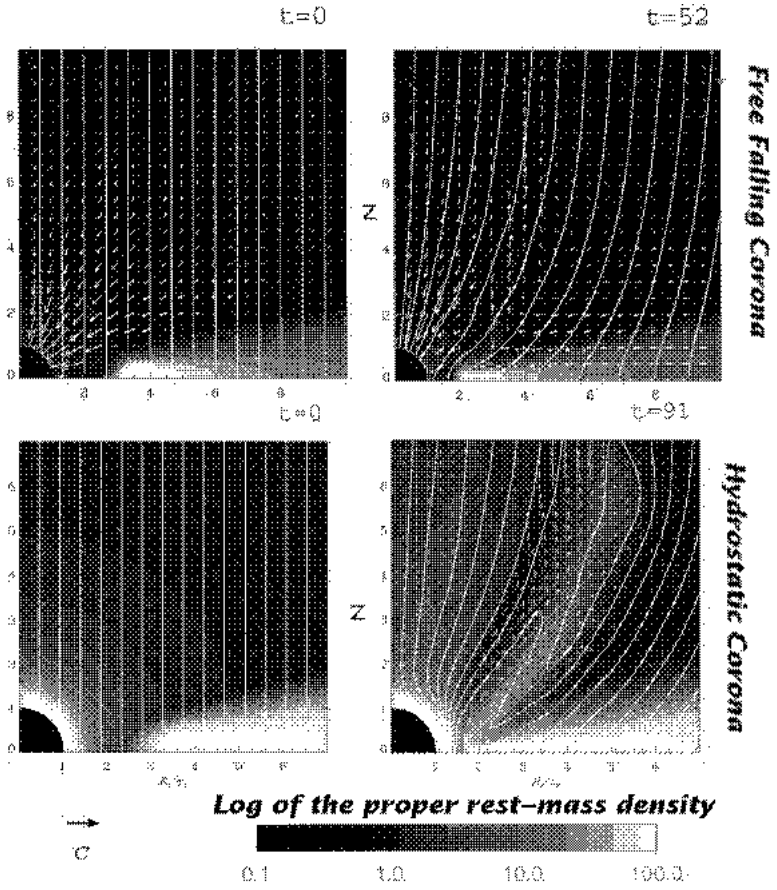

Fig. 6. Figure from [76]. Initial and final time snapshots of the logarithm of the density around a non rotating Schwarzschild BH. Top panels: free falling corona case. Bottom panels: hydrostatic corona case. The solid lines are the magnetic field lines. The vector plots show the flow velocity. On the initial state a uniform axial magnetic field is set up. The disk (in white color) rotates around the BH with Keplerian velocity. In the right panels the jet is formed almost along the magnetic field lines.

peak), which is characteristic of each GRB and usually is about several hundreds of keV. The observed fluence on earth is $10^{-5} - 10^{-7}$ erg/cm^2.

For years it was unclear whether GRBs take place at local or cosmological distances (see *e.g.*, [105]). However, a galactic origin can ve excluded, because the BATSE catalog shows an isotropic distribution of GRBs over the sky [104]. BeppoSAX spacecraft [29] has provided accurate coordinates ($\sim$ arc minutes) of the fading X–ray counterparts of GRBs, which has allowed for subsequent ground based observations of faint GRB afterglows at optical and radio wavelengths. The recent redshift determinations, obtained from the optical spectra, prove

the cosmological origin at least of the majority of GRBs (see [48] for more information). Observed redshift values are in the range $0.7 \leq z \leq 3.4$ implying emitted gamma-ray energies of $2 \times 10^{51} \leq E \leq 2.3 \times 10^{54}$ erg for an isotropically radiating source. The cosmological origin of the GRBs is consistent with the distribution of bursts in the $\log N - \log P$ plane.

Nonetheless, the accuracy of the positioning is neither sufficient to determine the host galaxies of GRBs nor their progenitors. This picture was challenged by the detection of the Type Ib/c supernova SN 1998bw [46,47] within the error box of GRB 980425 [149,126] whose explosion time and location is consistent with that of the GRB. This suggests a relationship between GRBs and SNe Ib/c, *i.e.,* core collapse supernovae of massive stellar progenitors which have lost their hydrogen and helium envelopes [47,66]. However, the observation of a second fading X–ray source within the error box of GRB 980425 (different from SN 1998bw) still causes some doubts on the GRB–supernova connection, although the probability of chance coincidence of GRB 980425 and SN 1998bw is almost negligible [126].

Another clue on the nature of the progenitors of GRBs comes from the duration of the shorter bursts and the temporal substructure of the longer bursts (~ 1 msec). If the time variation is intrinsic, the length scales involved in the production of a GRB are of about 1 light–millisecond, which in turn points towards compact objects, like NSs or BHs. Furthermore, the non recurrence of the events points towards cataclysmic astrophysical events.

The compact nature of GRB sources, the observed flux and the cosmological distance taken together imply a large photon density and, therefore, a large optical depth for pair production. This is, however, inconsistent with the optically thin source indicated by the non–thermal gamma–ray spectrum, which extends well beyond the pair production threshold at 0.5 MeV. This problem (*compactness problem*) can be resolved by assuming an ultra–relativistic expansion of the emitting region. The bulk Lorentz factor required are $\Gamma > 100$ (see, *e.g.,* [128])

Various catastrophic collapse events have been proposed in order to explain the energies released in a GRB. Among those proposals we find neutron–star/neutron–star mergers [120,52], neutron–star/black–hole mergers [108], collapsars [166,90] and hypernovae [121]. These models rely on the existence of a stellar mass BH hole which accretes several solar masses of matter from a disk (formed during a merger or by a non–spherical collapse) at a rate of $\sim 1\, M_\odot\, \mathrm{s}^{-1}$ [131]. A fraction of the gravitational binding energy released by accretion is converted into neutrino and anti–neutrino pairs, which in turn annihilate into electron–positron pairs. This creates a pair fireball, which will also include baryons present in the environment surrounding the black hole. If the baryon load (the ratio of the fireball mass to its energy) of the fireball is small enough, the baryons are accelerated together with the $\mathrm{e}^+\,\mathrm{e}^-$ pairs to ultra–relativistic speeds with Lorentz factors $> 10^2$ [23,129]. The existence of such relativistic flows is supported by radio observations of GRB 980425 [82]. The rapid temporal decay of several GRB afterglows is inconsistent with spherical (isotropic) blast wave models propagating through the interstellar medium, and

instead is more consistent with the evolution of a relativistic jet after it slows down and spreads laterally [137]. Finally, the bulk kinetic energy of the fireball is thought to be converted into gamma–rays via cyclotron radiation and/or inverse Compton processes (see, *e.g.*, [105,128]).

One–dimensional numerical simulations of spherically symmetric relativistic fireballs have been performed by several authors to model GRB sources (*e.g.*, [129,123,124,59]). Multi–dimensional modeling of ultra–relativistic jets in the context of GRBs has for the first time been attempted by Aloy *et al.* [7]. Using a collapsar progenitor model (from [90]) they have simulated the propagation of an axisymmetric jet through the mantle and envelope of a collapsing massive star using a version of GENESIS [3] that includes a background Schwarzschild metric. The jet forms as a consequence of an assumed energy deposition rate of $10^{50} - 10^{51}$ erg/sec within a 30° cone around the rotation axis. When the jet reaches the surface of the stellar progenitor, the maximum Lorentz factor attained by the flow is about 20. The latter fact implies that Newtonian simulations of this phenomenon [90] are clearly inadequate. The simulations also try to address the ulterior acceleration of the fireball when the jet propagates through an atmosphere of declining density. At the end of the simulations (when the jet has gone over $\sim 10^{11}$ cm) the maximum Lorentz factor is about 50 (for an energy deposition rate of 10^{51} erg/sec). The baryonic contamination is very heterogenous having an average value of 1. However, there are regions (coincident with the parts of the flow having the largest Lorentz factor) where this value is as small as 10^{-5}, which is in agreement with the theoretical expectations (see above). Although the final Lorentz factor is small compared with the predictions of the standard model [23,129], the distance up to which the jet propagation has been tracked (8×10^{10} cm) is much smaller than the one assumed to produce efficient internal shocks ($10^{12} - 10^{14}$ cm) and the fireball to become optically thin ($\sim 10^{13}$ cm, [128]). Therefore, there is still room for further acceleration of the jet until it becomes transparent. Finally, there are recent claims pointing to the possibility of GRB generation without extremely high Lorentz factors and with much smaller masses than in the standard model [153].

6 Summary

Hydrodynamic relativistic processes are on the basis of a variety of challenging astrophysical phenomena. On the other hand, relativistic astrophysics has benefited of the recent development of accurate numerical techniques which have allowed, for the first time, the simulation of ultrarelativistic multidimensional flows. Two main applications are currently addressed. One is in the field of relativistic jets, where very important advances have been made in problems like the jet formation mechanisms or the nature of superluminal sources. The other main application is in the field of GRBs. In order to stress the importance of relativistic hydrodynamic simulations in these fields, let us remind that the generation of both relativistic jets and GRBs is hidden to present observations making numerical simulations the only means to confront the theoretical models.

In the present review we have rewritten the equations governing the dynamics of relativistic perfect fluids paying special attention to their conservative and hyperbolic character (two properties which are extensively exploited by modern numerical techniques). We have also reviewed the evolution of numerical relativistic hydrodynamics, that started as a branch of relativistic astrophysics more than thirty years ago with the pioneering simulations of May and White of stellar core collapse, and which has culminated in the last decade with the introduction of high–resolution shock–capturing (HRSC) methods. The basics of HRSC methods have been summarized, too.

Most of the problems that may be treated by means of numerical simulations require a multidimensional modeling of the flows. Fully three–dimensional simulations in relativistic hydrodynamics are particularly challenging because of their intrinsic, technical difficulties. These difficulties have been addressed only by a few scientific groups, so far. We have listed those codes that have been used in 3D special or general RHD simulations. Two of them (Cactus and Shibata–Nakamura codes) have implemented a full consistent evolution of the metric of the space–time coupled to the GRHD equations. This fact has allowed them to study, for the first time, problems as complex as the coalescence of simplified models of NSs. The other two codes (GENESIS and Koide codes) allow for a static background metric of the space–time and even for the inclusion of the magnetic field in the equations (Koide's code).

The last Section has been devoted to outline the main results in the simulation of relativistic extragalactic jets and GRBs.

Acknowledgements

This work has been supported in part by the Spanish DGES (grant PB 97-1432). M.A. Aloy thanks to MPA for financial support under its guest program and to the Spanish MEC for the a grant (EX 00 22566499). The authors thank J.M. Ibáñez and E. Müller for the critical reading of the manuscript.

References

1. C.E. Akujor: Astron. Astrophys. **259**, L61 (1992)
2. M. Alcubierre, B. Bruegmann, *et al.*:Phis. Review D **62**, 044034 (2000)
3. M.A. Aloy, J.M^{a}. Ibáñez, J.M^{a}. Martí, E. Müller: Astrophys. J. Suppl. **122**, 151 (1999)
4. M.A. Aloy, J.M^{a}. Ibáñez, J.M^{a}. Martí, J.L. Gómez, E. Müller: Astrophys. J. Lett. **523**, L125 (1999)
5. M.A. Aloy, J. Pons, J.M^{a}. Ibáñez, Comput. Phys. Commun. **120**, 115 (1999)
6. M.A. Aloy, J.M^{a}. Ibáñez, J.M^{a}. Martí, J.L. Gómez, E. Müller: Astrophys. J. Lett. **528**, L85 (2000)
7. M.A. Aloy, E. Müller, J.M^{a}. Ibáñez, J.M^{a}. Martí, A. MacFadyen: Astrophys. J. Lett. **531**, L119 (2000)
8. A.M. Anile. *Relativistic Fluids and Magnetofluids*, (Cambridge University Press, Cambridge 1989)
9. R. Arnowitt, S. Deser, C.W. Misner. *Gravitation: An Introduction to Current Research*, ed., Witten, L., (John Wiley, New York, 1962) p. 227
10. J.M. Attridge, D.H. Roberts, J.F.C. Wardle: Astrophys. J. Lett. **518**, L87 (1999)

11. D.S. Balsara: J. Comp. Phys. **114**, 284 (1994)
12. F. Banyuls, J.A. Font, J.M^{a}. Ibáñez, J.M^{a}. Martí, J.A. Miralles: Astrophys. J. **476**, 221 (1997)
13. M.C. Begelman, R.D. Blandford, M.J. Rees: *Rev. Mod. Phys.*, **56**, 255 (1984)
14. M.C. Begelman, M.J. Rees, M. Sikora: Astrophys. J. Lett. **429**, L57 (1994)
15. M.J. Berger, P. Colella: J. Comp. Phys. **82**, 64 (1989)
16. G.V. Bicknell. In *Energy Transport in Radio Galaxies and Quasars*, eds. P.E. Hardee, A.H. Bridle, J.A. Zensus. (ASP Conference Series, 1996) **100**, p. 253
17. R.D. Blandford. In *Active Galactic Nuclei*, eds. T.K.-L. Courvoisier and M. Mayor (Springer, Berlin, 1990), p. 161
18. R.D. Blandford, D.G. Payne: Mon. Not. Roy. Astronom. Soc. **199**, 883 (1982)
19. R.D. Blandford, M.J. Rees: Mon. Not. Roy. Astronom. Soc. **169**, 395 (1974)
20. J.P. Boris, D.L. Book: J. Comp. Phys. **11**, 38 (1973)
21. A.H. Bridle, D.H. Hough, *et al.*: Astronom. J. **108**, 766 (1994)
22. More information can be found under the URL: `http://www.cactuscode.org`.
23. G. Cavallo, M.J. Rees: Mon. Not. Roy. Astronom. Soc. **183**, 359 (1978)
24. J. Centrella, J.R. Wilson: Astrophys. J. **54**, 229 (1984)
25. A.J. Chorin: J. Comp. Phys. **22**, 517 (1976)
26. E. Chow, J.J. Monaghan: J. Comp. Phys. **134**, 296 (1997)
27. P. Colella: SIAM J. Sci. Comput. **3**, 76 (1982)
28. P. Colella, P.R. Woodward: J. Comp. Phys. **54**, 174 (1984)
29. E. Costa, *et al.*: Nature **387**, 783 (1997)
30. R. Courant, K.O. Friedrichs. *Supersonic Flows and Shock Waves*, (Springer, Berlin 1976)
31. W. Dai, P.R. Woodward: SIAM J. Sci. Comput. **18**, 982 (1997)
32. S.F. Davis: *ICASE Report No. 84–20* (1984)
33. G.C. Duncan, P.A. Hughes: Astrophys. J. Lett. **436**, L119 (1994)
34. G.C. Duncan, P.A. Hughes, J. Opperman. In *Energy Transport in Radio Galaxies and Quasars*, eds. P.E. Hardee, A.H. Bridle and J.A. Zensus, ASP Conference Series (1996), **100**, p. 143-148
35. R. Donat, J.M. Font, J.M^{a}. Ibáñez, A. Marquina: J. Comp. Phys. **146**, 58 (1998)
36. R. Donat, A. Marquina: J. Comp. Phys. **125**, 42 (1996)
37. B. Einfeldt: SIAM J. Numer. Anal. **25**, 294 (1988)
38. F. Eulderink, G. Mellema: Astron. Astrophys. **284**, 654 (1994)
39. F. Eulderink, G. Mellema: Astron. Astrophys. Suppl. **110**, 587 (1995)
40. C.R. Evans. In *Dynamical Space–Times and Numerical Relativity*, ed. J. Centrella, (Cambridge University Press, Cambridge, 1986) p. 3
41. S.A.E.G. Falle, S.S. Komissarov: Mon. Not. Roy. Astronom. Soc. **278**, 586 (1996)
42. B.L. Faranoff, J.M. Riley: Mon. Not. Roy. Astronom. Soc. **167**, 31 (1974)
43. J.A. Font, J.M^{a}. Ibáñez, J.M^{a}. Martí, A. Marquina: Astron. Astrophys. **282**, 304 (1994)
44. J.A. Font, M. Miller, W.-M. Suen, M. Tobias: *Phys. Rev.* **D** 61, 044011 (1999)
45. J.A. Font, *Living Reviews in Relativity* (2000), under the URL: `http://www.livingreviews.org/Articles/Volume3/2000-2font`
46. T.J. Galama, P.M. Vreeswijk, E. Pian, F. Frontera, V. Doublier, J.-F. Gonzalez: *IAU Circ.*, 6985 (1998)
47. T.J. Galama, P.M. Vreeswijk, *et al.*: Nature **395**, 670 (1998)
48. T.J. Gallama, (2000), this volume.
49. G. Ghisellini, P. Padovani, A. Celotti, L. Maraschi: Astrophys. J. **407**, 65 (1993)
50. J. Glimm: Comm. Pure Appl. Math. **18**, 697 (1965)

51. S.K. Godunov: *Mat. Sb.*, **47**, 271 (1959)
52. J. Goodman: Astrophys. J. Lett. **308**, L47 (1986)
53. J.L. Gómez, A. Alberdi, J.M. Marcaide: Astron. Astrophys. **274**, 55 (1993)
54. J.L. Gómez, A. Alberdi, J.M. Marcaide: Astron. Astrophys. **284**, 51 (1994)
55. J.L. Gómez, J.M$^{\underline{a}}$. Martí, A.P. Marscher, J.M$^{\underline{a}}$. Ibáñez, J.M. Marcaide: Astrophys. J. Lett. **449**, L19 (1995)
56. J.L. Gómez, J.M$^{\underline{a}}$. Martí, A.P. Marscher, J.M$^{\underline{a}}$. Ibáñez, A. Alberdi: Astrophys. J. Lett. **482**, L33 (1997)
57. J.L. Gómez, A.P. Marscher, A. Alberdi, D.C. Gabuzda: Astrophys. J. **519**, 642 (1999)
58. J.L. Gómez, (2000), this volume.
59. J. Granot, M. Miller, T. Piran, W.-M. Suen. In *Gamma–Ray Bursts*. Eds. R.M. Kippen, R.S. Mallozzi and G.J. Fishman, (AIP conference proceedings 2000), **526**, 540.
60. A. Harten: *Comp. Pure Appl. Math.* **48**, 12 (1995)
61. A. Harten: SIAM J. Numer. Anal. **21**, 1 (1984)
62. A. Harten, B. Engquist, S. Osher, S. Chakravarthy: J. Comp. Phys. **71**, 231 (1987)
63. J.F. Hawley, L.L. Smarr, J.R. Wilson: Astrophys. J. Suppl. **55**, 211 (1984)
64. J.R.A. Hooimeyer, P.D. Barthel, R.T. Schilizzi, G.K. Miley: Astron. Astrophys. **261**, 25 (1992)
65. C.A. Hummel, *et al.*: Astron. Astrophys. **257**, 489 (1992)
66. T.J. Iwamoto, P.A. Mazzali, *et al.*: Nature **395**, 672 (1998)
67. T.W. Jones. In *Supermassive black holes*, (Cambridge University Press, Cambridge 1988), p. 59
68. T.W. Jones, S.L. O'Dell: Astrophys. J. **214**, 522 (1977)
69. W. Junor, J.A. Bireta: Astronom. J. **109**, 500 (1995)
70. A. Kheyfets, W.A. Miller, W.H. Zurek: *Phys. Rev. D* **41**, 451 (1990)
71. R.W. Klebesadal, I.B. Strong, R.A. Olsen: Astrophys. J. Lett. **182**, L85 (1973)
72. A. Königl: Astrophys. J. **243**, 700 (1981)
73. S. Koide: Astrophys. J. **487**, 66 (1997)
74. S. Koide, K.-I. Nishikawa, R.L. Muttel: Astrophys. J. Lett. **463**, L71 (1996)
75. S. Koide, K. Shibata, T. Kudoh: Astrophys. J. Lett. **495**, L63 (1998)
76. S. Koide, K. Shibata, T. Kudoh: Astrophys. J. **522**, 727 (1999)
77. S. Koide, D.L. Meier, K. Shibata, T. Kudoh: Astrophys. J. **536**, 668 (2000)
78. S.S. Komissarov: *Sov. Astron. Lett.* **16**(4), 284 (1990)
79. S.S. Komissarov, S.A.E.G. Falle: Mon. Not. Roy. Astronom. Soc. **288**, 833 (1997)
80. S.S. Komissarov, S.A.E.G. Falle: Mon. Not. Roy. Astronom. Soc. **297**, 1087 (1998)
81. A.K. Kembhavi, J.V. Narlikar. *Quasars and Active Galactic Nuclei. An introduction* (Cambridge University Press, Cambridge 1999)
82. S.R. Kulkarni, D.A. Frail, *et al.*: Nature **395**, 663 (1998)
83. P. Laguna, W.A. Miller, W.H. Zurek: Astrophys. J. **404**, 678 (1993)
84. N.K. Lahy, N.K. *A Particle Method for Relativistic Fluid Dynamics*, M.Sc. Thesis, Monash University (1989)
85. R.A. Laing. In *Radio Galaxies and Quasars*, eds. P.E. Hardee, A.H. Bridle, J.A. Zensus. ASP Conference Series, Vol. 100 (1996) p. 241
86. W. Landry, S.A. Teukolsky: submitted (1999). See also: gr-qc/9912004
87. R.J. LeVeque. *Numerical Methods for Conservation Laws*, 2nd. edn. (Birkhäuser, Basel 1992)
88. A.P. Lovanov, T.P. Krichbaum, *et al.*: Astron. Astrophys. **340**, L60 (1998)
89. L.B. Lucy: Astronom. J. **82**, 1013 (1977)

90. A. MacFadyen, S.E. Woosley: Astrophys. J. **524**, 262 (1999)
91. P.J. Mann: Comput. Phys. Commun. **67**, 245 (1991)
92. P.J. Mann: Comput. Phys. Commun. **107**, 188 (1993)
93. A. Marquina: SIAM J. Sci. Comput. **15**, 892 (1994)
94. A.P. Marscher: Astrophys. J. **235**, 386 (1980)
95. A.P. Marscher, W.K. Gear: Astrophys. J. **298**, 114 (1985)
96. A.P. Marscher, W.K. Gear, J.P. Travis. In *Variability of Blazars*, ed. by E. Vataoja and M. Valtonen (Cambridge University Press, Cambridge 1992)
97. J.M$^{\underline{a}}$. Martí, J.M$^{\underline{a}}$. Ibáñez, J.A. Miralles: Phis. Review D **43**, 3794 (1991)
98. J.M$^{\underline{a}}$. Martí, E. Müller: J. Fluid Mech. **258**, 317 (1994)
99. J.M$^{\underline{a}}$. Martí, E. Müller, J.M$^{\underline{a}}$. Ibáñez: Astron. Astrophys. **281**, L9 (1994)
100. Martí, J.M$^{\underline{a}}$, E. Müller, J.A. Font, J.M$^{\underline{a}}$. Ibáñez: Astrophys. J. **448**, L105 (1995)
101. Martí, J.M$^{\underline{a}}$, Müller, E., J.A. Font, J.M$^{\underline{a}}$. Ibáñez, A. Marquina: Astrophys. J. **479**, 151 (1997)
102. J.M$^{\underline{a}}$, Martí, E. Müller: *Living reviews in Relativity* (1999), under the URL: `http://www.livingreviews.org/Articles/Volume2/1999-3marti`
103. M.M. May, R.H. White: *Methods Comput. Phys.* **7**, 219 (1967)
104. C.A. Meegan, G.J. Fishman, *et al.*: Nature **355**, 143 (1992)
105. P. Mèszáros. In *Proc. of the 17th Texas Symp. on Relativistic Astrophysics and Cosmology*, eds. H. Böhringer, G.E. Morfill and J.E. Trümper, (N. Y. Acad. Sci., 1995) p. 440
106. A.J. Mioduszewski, P.A. Hughes, G.C. Duncan: Astrophys. J. **476**, 649 (1997)
107. I.F. Mirabel, L.F. Rodriguez: Nature **371**, 46 (1994)
108. R. Mochkovitch, M. Hernanz, J. Isern, X. Martin: Nature **361**, 236 (1993)
109. J.J. Monaghan: Comput. Phys. Rep. **3**, 71 (1985)
110. J.J. Monaghan: J. Comp. Phys. **136**, 298 (1997)
111. T. Nakamura: Prog. Theor. Phys. **65**, 1876 (1981)
112. T. Nakamura, K. Oohara, Y. Kojima: Prog. Theor. Phys. Suppl. **90**, 76 (1987)
113. T. Nakamura, K. Oohara. In *Numerical Astrophysics*. Ed. by S.M. Miyama, K. Tomisaka and T. Hanawa (Kluwer Academic, Astrophysics and space science library 1999) **240**, p.247
114. T. Nakamura, K. Maeda, S. Miyama, M. Sasaki: Prog. Theor. Phys. **63**, 1229 (1980)
115. K.-I. Nishikawa, S. Koide, *et al.*: Astrophys. J. **483**, L45 (1997)
116. K.-I. Nishikawa, S. Koide, *et al.*: Astrophys. J. **498**, 166 (1998)
117. M.L. Norman, L. Smarr, K.-H.A. Winkler, M.S. Smith: Astron. Astrophys. **113**, 285 (1982)
118. M.L. Norman, K.-H.A. Winkler. In: *Astrophysical Radiation Hydrodynamics*, ed. by M.L. Norman, K.-H.A. Winkler (Reidel, Dordrecht, 1986) p. 227
119. S. Osher, S. Chakravarthy: SIAM J. Numer. Anal. **21**, 995 (1984)
120. B. Pacyński: Astrophys. J. **308**, L43 (1986)
121. B. Pacyński: Astrophys. J. **494**, L45 (1998)
122. A. Panaitescu, L. Wen, P. Laguna, P. Mészáros: Astrophys. J. **482**, 942 (1999)
123. A. Panaitescu, P. Mészáros: Astrophys. J. **492**, 683 (1998)
124. A. Panaitescu, P. Mészáros: Astrophys. J. **526**, 707 (1999)
125. L.I. Petrich, S.L. Shapiro, R.F. Stark, S.A. Teukolsky: Astrophys. J. **336**, 313 (1989)
126. E. Pian, L. Amati, *et al.*: Astrophys. J. **538**, 638 (2000)
127. T. Piran: J. Comp. Phys. **35**, 254 (1980)
128. T. Piran: *Physics Reports* **314**, 575 (1999)

129. T. Piran, A. Shemi, R. Narayan: Mon. Not. Roy. Astronom. Soc. **263**, 861 (1993)
130. J.A. Pons, J.Mª Martí, E. Müller: J. Comp. Phys. **422**, 125 (2000)
131. R. Popham, S.E. Woosley, C. Fryer: Astrophys. J. **518**, 356 (1999)
132. P.L. Roe: J. Comp. Phys. **43**, 357 (1981)
133. R.D. Richtmyer, K.W. Morton: *Difference Methods for Initial–value Problems*, (Wiley–Interscience, New York 1967)
134. Rosen, A., Hughes, *et al.*: Astrophys. J. **516**, 729 (1999)
135. C. Sauty (2000), this volume.
136. R.H. Sanders, K.H. Prendergast: Astrophys. J. **188**, 489 (1974)
137. R. Sari, T. Piran, J.P. Halpern: Astrophys. J. Lett. **519**, L17 (1999)
138. P.A.G. Scheuer: Mon. Not. Roy. Astronom. Soc. **166**, 513 (1974)
139. V. Schneider, U. Katscher, *et al.*: J. Comp. Phys. **105**, 92 (1993)
140. M. Shibata, T. Nakamura: Phis. Review D **52**, 5428 (1995)
141. M. Shibata: Prog. Theor. Phys. **101**, 251 (1999)
142. M. Shibata: Prog. Theor. Phys. **101**, 1199 (1999)
143. M. Shibata: Phis. Review D **60**, 104052 (1999)
144. M. Shibata, T.W. Baumgarte, S.L. Shapiro: Phis. Review D **61**, 044012 (2000)
145. S. Siegler, H. Riffert: Astrophys. J. Suppl. **531**, 1053 (2000)
146. C.W. Shu: *Math. Comp.* **49**, 105 (1987)
147. C.W. Shu, S.J. Osher: J. Comp. Phys. **83**, 32 (1989)
148. L. Smarr, J.R. Wilson, R.T. Barton, R.L. Bowers: Astrophys. J. **246**, 515 (1981)
149. P. Soffitta, M. Feroci, *et al.*: *IAU Circ.* 6884 (1998)
150. J. Sollfrank, P. Huovinen, M. Kataja, P.V. Ruuskanen, M. Prakash, R. Venugopalan: *Phys. Rev. C* **55**, 392 (1997)
151. R.F. Stark, T. Piran: Comput. Phys. Rep. **5**, 221 (1987)
152. M.R. Swain, A.H. Bridle, S.A. Baum: Astrophys. J. **507**, L29 (1998)
153. J.C. Tan, C.D. Matzner, C.F. McKee: Astrophys. J. , submitted, (2000)
154. M. Taub: *Phys. Rev.* **74**, 328 (1948)
155. K.W. Thomson: J. Fluid Mech. **171**, 365 (1986)
156. S.J. Tingay, D.L. Jauncey, R.A. Preston, J.E. Reynolds, D.L. Meier *et al.*: Nature **374**, 141 (1995)
157. E. Toro: *Riemann solvers and numerical methods for fluid dynamics: a practical introduction*, 1st edn. (Springer, Berlin 1997)
158. B. van Leer: J. Comp. Phys. **32**, 101 (1979)
159. M.H.P.M. van Putten: J. Comp. Phys. **105**, 339 (1993a)
160. M.H.P.M. van Putten: Astrophys. J. Lett. **408**, L21 (1993b)
161. M.H.P.M. van Putten: Astrophys. J. Lett. **467**, L57 (1996)
162. J. von Neumann, R.D. Richtmyer: *J. Appl. Phys.* **21**, 232 (1950)
163. L. Wen, A. Panaitescu, P. Laguna: Astrophys. J. **486**, 919 (1997)
164. J.R. Wilson: Astrophys. J. **173**, 431 (1972)
165. J.R. Wilson. In: *Sources of Gravitational Radiation*, ed. by L.L. Smarr, (Cambridge University Press, Cambridge 1979) p. 423
166. S.E. Woosley: Astrophys. J. **405**, 273 (1993)
167. Yang, J.Y., Chen, M.H., Tsai, I-N. and J.W. Chang: J. Comp. Phys. **136**, 19 (1997)